# Polyvinyl Alcohol Scaffold Incorporated with Silver Nanoparticles and Titanium Dioxide: Electrical, Dielectric, Dye Degradation, and Antibacterial Properties


**Joel Saji, Akhela Umapathi, S. R. Manohara, P. N. Navya, Mamta Kumawat, Divya Prakash, and Hemant Kumar Daima**

**Abstract** The importance of nanomaterials which can be easily incorporated into the polymeric scaffolds is growing for their potential applications. Therefore, in the present work, we have developed different polymeric scaffolds based on the polyvinyl alcohol (PVA) matrix. The PVA scaffold is integrated with tyrosine-capped silver (Ag) nanoparticles, titanium dioxide ($TiO_2$), pristine tyrosine, and pristine $Ag^+$ ions. The dielectric properties (dielectric constant, dielectric loss, and tangent loss) and AC electrical conductivity of PVA and its scaffold-integrated materials have been investigated as a function of frequency at room temperature. The dielectric studies show low values of dielectric constant and dielectric loss in the studied frequency range. The potential dye-degradation activity and antibacterial action was also assessed toward malachite green and Gram-negative *Escherichia coli*, respectively. The composition of the scaffold is important in determining the malachite green degradation and in inhibiting the Gram-negative bacterial growth. This work shows that suitable integration of nanomaterials within the matrix can find applications in various fields including dye degradation, antimicrobial agents, energy storage, and flexible electronics.

J. Saji · D. Prakash (✉)
Amity School of Applied Sciences, Amity University Rajasthan, Jaipur 303002, Rajasthan, India

J. Saji · A. Umapathi · M. Kumawat · H. K. Daima
Amity Center for Nanobiotechnology and Nanomedicine (ACNN), Amity Institute of Biotechnology, Amity University Rajasthan, Jaipur 303002, Rajasthan, India
e-mail: hkdaima@jpr.amity.edu

S. R. Manohara
Nano-Composites and Materials Research Lab, Department of Physics, Siddaganga Institute of Technology, Tumakuru 572103, Karnataka, India

P. N. Navya
Department of Biotechnology, Bannari Amman Institute of Technology, Sathyamangalam, Erode 638401, Tamil Nadu, India

D. Prakash
SBES Shobhit University, Gangoh, Adarsh Institutional Area, Babu Vijendra Marg, Gangoh, Saharanpur, Uttar Pradesh 247341, India



G. Manik et al. (eds.), *Advances in Mechanical Engineering*, Lecture Notes in Mechanical Engineering, https://doi.org/10.1007/978-981-16-0942-8_36

**Keywords** PVA scaffold/matrix · Silver nanoparticles · Titanium dioxide · Dielectric · Dye degradation · Antibacterial

## 1 Introduction

The rise in the demand for synthetic dyes in pulp and paper, distilleries and tanneries, leather, paint and textile industries led to elevation in synthetic dyes production, and ~1–1.5 tons of the dyes are globally released into the environment [1], in which textile industry is the major contributor [2–4]. This has caused serious concerns on the surface and ground waters, and it is affecting the fauna and flora [5]. Further, the presence of pathogenic microorganisms in the contaminated water causes serious gastrointestinal diseases [6]. Moreover, most of the synthetic dyes are stable organic molecules, and they may be persisting in the environment for longer time, which can even pass through food chain to become carcinogenic due to their chemical nature [7–9].

The anthraquinone, arylmethane, azo, indigoid, phthalocyanine, and xanthane class of dyes are recurrently used for industrial purposes [10]. Among them, malachite green, a triarylmethane group, and anionic dye is used in aquaculture, food additive, cosmetics, leather, paint, and textile industries for its fungicidal, parasiticide, antiprotozoal, and antibacterial nature. However, the industrial malachite green enters the body in ionic form which is aided by their high lipid solubility to cause severe toxicity and bioaccumulation in the humans. With a tolerance limit of 0.1 mg/kg in the human body, malachite green acts a multi-organ toxin having undesirable effects on liver, spleen, kidney, urinary bladder, heart, and thyroid follicles [11]. Furthermore, malachite green is known to cause teratogenicity, mutagenesis, chromosomal fracture, and respiratory toxicity [12, 13]. To aggravate, the toxicity of the malachite green increases with the raise in the temperature [11]. However, high-frequency usage of malachite green continues despite being banned in many countries due to its highly effective and economical nature.

In the context of above, the conventional methods for removal of dyes are based on chemical, physical, or biological procedures [14–18]; however, these are having several limitations such as high-priced, low efficiency, inferiorly versatile, and their waste-disposal (wherein the treatment is incompetent for full degradation of stable synthetic dyes) [19, 20]. One of the most effective methods developed recently includes titanium dioxide ($TiO_2$)-mediated degradation, which is an active photocatalyst, and known to be biologically/chemically inert [21–23]. Furthermore, the nanotechnological-based solutions are the state-of-the-art resolutions to degradation problems due to the large surface area and unique features influenced by the size, surface structure, and shape of the synthesized nanoparticles.

In recent years, the incorporation of metal nanoparticles into polymer matrices have gained much attention for their remarkable applications, and silver (Ag) nanoparticles are at the forefront due to their unique catalytic, optical, electrical, and antibacterial properties. Ag nanoparticle-based catalytic systems are gaining great

attention because of their stability, selectivity, and reactivity [24]. The efficiency of the degradation can be further improved in the visible region by fine-tuning their physicochemical properties [25–27].

Therefore, in the present study, different films have been developed by incorporating $TiO_2$, and Ag nanoparticles in PVA scaffold. PVA is a hydrophilic polymer, and it acts as a membrane to entrap $TiO_2$, Ag nanoparticles, and other pristine molecules. This newly prepared hybrid membrane composite materials are active combination of polymer, $TiO_2$ and nanoparticles, and they are expected to improve the mechanical properties, fire resistance capabilities, biocompatibility, and other factors of the polymer. The hybrid polymer matrices are found to have better catalytic activity than colloidal Ag nanoparticles due to stability and uniform dispersity [26], and they are reported to degrade many organic pollutants including synthetic dyes [28–31]. The pollutants degradation and antimicrobial potential of hybrid polymer matrices are due to a series of reactions caused and mediated by hydroxyl radicals [32, 33].

Therefore, we have evaluated the photocatalytic degradation of malachite green dye, antibacterial property against *Escherichia coli*, and assessed the electrical and dielectric properties in the frequency range from 50 to 8 MHz at room temperature for conductance capacity of the prepared hybrid films.

## 2 Materials and Methods

### *2.1 Materials*

Potassium hydroxide (KOH), L-tyrosine, poly vinyl alcohol (PVA, MW 893.

,000–98,000), silver nitrate ($AgNO_3$), and titanium dioxide ($TiO_2$) were purchased from Sigma-Aldrich, and malachite green was purchased from Qualigens Fine Chemicals. All the chemicals were of analytical grade and were used as received. Milli-Q water of 18.2 MΩ cm resistivity at 25 °C was used to prepare all the solutions and growth media. All the glass-wares were thoroughly washed with aqua regia (mixture of HCl and $HNO_3$) before use.

### *2.2 L-tyrosine Synthesized Silver (Ag) Nanoparticles*

The protocol followed for the preparation of Ag nanoparticles is as described in [34], wherein a 100 ml solution consisting of L-tyrosine (0.1 mM) and KOH (1 mM) was allowed to warm at 70 °C. The $AgNO_3$ (0.2 mM) was added drop by drop, and the heating was turned off when the solution turned yellow. The nanoparticles solution was kept under continuous stirring at room temperature, followed by slow heating

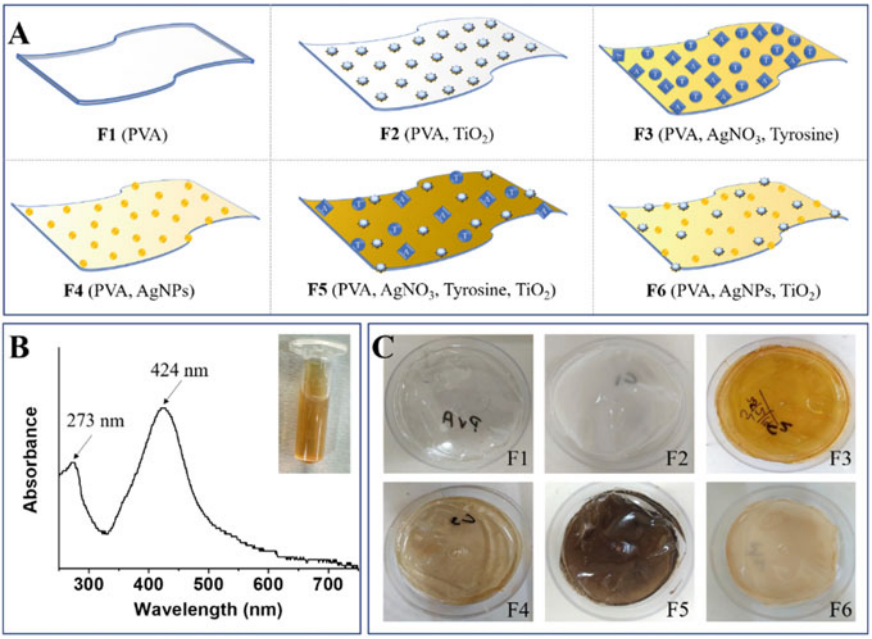


**Fig. 1** Schematic representation of different PVA scaffold-based films (F1–F6) with various compositions incorporating $AgNO_3$, $TiO_2$, Ag nanoparticles (AgNPs) and tyrosine amino acid (Panel A). The UV–visible spectroscopic analysis of tyrosine synthesized Ag nanoparticles and their optical image showing characteristic yellow color of Ag nanoparticles (Panel B). The digital photographs of various composite films, wherein, the incorporation of $AgNO_3$, $TiO_2$, Ag nanoparticles, and tyrosine have imparted various colors (Panel C)

to evaporate water from the nanoparticles solution to increase the Ag metal concentration 5X. The concentrated Ag nanoparticles solution was used to incorporate in PVA scaffold (Fig. 1, F4 and F6).

## *2.3 Preparation of PVA and PVA Based Scaffolds by Incorporation of $AgNO_3$,* L*-tyrosine, AgNPs, and $TiO_2$*

In a typical experiment, 1.5 g of PVA powder was dissolved in MilliQ water, and the volume was made up to 30 mL. The solution was continuously stirred at 40 °C for 30 min, and the viscous solution was poured into a circular plate. After oven dry for 4 h, the obtained film was separated from the circular plate and named as F1 (Fig. 1).

Likewise, in the viscous solution of PVA, 2.5 mL of 0.1 M $TiO_2$ (Fig. 1, F2) or 2.5 mL of 1 mM $AgNO_3$/2 drops of L-tyrosine (0.01 mM) (Fig. 1, F3) or 2.5 mL of Ag nanoparticles (Fig. 1, F4) or 2.5 mL of 100 mM $TiO_2$/2.5 mL of 1 mM $AgNO_3$/few drops of L-tyrosine (0.01 mM) (Fig. 1, F5) or 2.5 mL of 100 mM $TiO_2$/2.5 mL of

Ag nanoparticles (Fig. 1, F6) were added to secure different films. The total volume of the reaction solutions in all the cases was maintained 30 mL.

## 2.4 Electrical and Dialectical Properties of the Films

The dielectric properties and AC electrical conductivities of the pure PVA scaffold (F1) and composites-PVA scaffolds (F2-F5) were measured using high precision LCR meter [Make: Hioki, Japan; Model: IM3536] in the frequency range from 50 Hz to 8 MHz using two-probe technique. The samples were cut in the form of circular disks of diameter 13 mm, and silver electrodes were provided on both sides of the sample for the measurement of their electrical and dielectric properties. The calculations of the dielectric constant, dielectric loss, loss tangent, and AC conductivity are presented elsewhere [35].

## 2.5 Evaluation of Dye Degradation Capacity

The dye degradation properties of the PVA based scaffolds (F1–F6) were assessed in time-dependent manner for malachite green through spectroscopic measurements. In a typical experiment, 3 mL of the dye malachite green, with the initial concentration of 10 mg/L was taken, and 1cm$^2$ respective scaffolds were placed into the vials. The dye solution and dye vials containing scaffolds were irradiated with a UV light of 270 nm, followed by collection of 200 µl of solutions at 0, 1, 3, 5, and 7 h, respectively. The absorbance was measured at a maximum wavelength of 618 nm for malachite green by using UV–vis spectrophotometer (Bio Mate 3S, Thermo Scientific, Massachusetts, USA), and the % degradation was calculated.

$$\text{Percentage (\%) dye degradation} = \frac{(A - A_0)}{A_0} \times 100 \quad (1)$$

where $A_0$ is initial absorbance and $A$ is absorbance after treatment. The experiments were performed in triplicates and error expressed as mean ± SE.

## 2.6 Assessment of Antimicrobial Potential of the Composite Scaffolds

The antimicrobial potency of the PVA based scaffolds (F1–F6) were assessed toward Gram-negative bacteria *Escherichia coli*. Typically, 100 µl culture from the overnight grown fresh culture with the absorbance of 1.48 was inoculated into the 30 mL nutrient broth, and 1 cm$^2$ respective films were placed into the flask. The flask from

the same bacterial culture without any treatment was considered control under similar experimental conditions. The absorbance at 600 nm was recorded at an interval of 2 h until the stationary phase was attained, and bacterial growth curve was constructed.

## 3 Results and Discussion

In the present work, PVA has been chosen as the scaffold because it is hydrophilic, biodegradable, and relatively stable polymer [36]. To this, tyrosine-capped Ag nanoparticles and $TiO_2$ were introduced to develop PVA based composite scaffolds. As shown in Fig. 1c, various free-standing films were prepared, and all of them have different color due to variety of compositions. The pure PVA membrane (Fig. 1c, F1) appears transparent, whereas $TiO_2$ containing film emerged as semi-transparent milky-white color (Fig. 1c, F2). The PVA polymer chains are most likely bound to the free $TiO_2$ through hydrogen bonds [37, 38]. The Ag nanoparticles or $Ag^+$ comprising films appeared in distinct colors ranging from light brown to dark brown due to differential composition of the membrane components. The films F3 and F5 developed yellow and dark yellow colors due to in-situ formation of the Ag nanoparticles by the reduction of $Ag^+$ through tyrosine, respectively. The similar in-situ Ag nanoparticles synthesis has been reported with polyetherimide using dimethylformamide as a reducing agent to improve the mechanical and electrical properties of the film [39]. The ex-situ formed tyrosine-capped Ag nanoparticles were also incorporated into the PVA scaffolds (Fig. 1c, F4 and F6). Previously, we have reported that phenolic group of tyrosine acts as a reducing agent to form Ag nanoparticles, which are capped with the oxidized tyrosine molecules [40–43]. Moreover, it has been reported that the PVA nanofibers interact with the Ag nanoparticles through the OH groups present in the PVA [44]. When tyrosine-coated Ag nanoparticles were added to the PVA, the interaction might be stimulated through the formation of hydroxy-1,4-benzoquinone like structures. Further, it has been indicated that island like structures will be developed on the addition of citrate-coated Ag nanoparticles within the $TiO_2$ sheets which are in nanometric size [45]. Since the interaction between Ag nanoparticles and $TiO_2$ is directed by the characteristics of the surface coating of the nanoparticles, we can expect similar interaction between tyrosine and $TiO_2$ which may influence the appearance of the PVA based films. In this study, the scaffolds were found to be stable at 50 °C for more than a year. Further, no visible aggregation was observed indicating the uniform distribution of the nanoparticles and $TiO_2$ moieties within the scaffolds. During the incorporation, it was observed that polymer matrix thereby prevented the nanoparticles from aggregation [26].

The UV–visible absorbance spectra of Ag nanoparticles showed an SPR band with maxima at 424 nm, which is consequent to metallic Ag as shown in Fig. 1b. An additional absorbance feature at 273 nm is originating due to the molecular transitions within Ag-attached oxidized tyrosine. The UV–visible spectroscopy of Ag nanoparticles further indicated that there was no aggregation in the particles, and they were found to be stable over a year in the solutions under standard laboratory

conditions (Fig. 1b). As shown in Fig. 1b, the solution color of the Ag nanoparticles was yellow, which is a typical characteristic of Ag nanoparticles. This further provided visible evidence that the nanoparticles are stable in nature, and there is no visible indication on aggregation.

The study of electrical and dielectric properties of such nanoparticles and $TiO_2$ moieties incorporated in to the PVA scaffolds is important, and therefore, we have investigated these physical properties as well. The frequency dependence of dielectric constant, $\varepsilon'$, of pure PVA and PVA-nanocomposite scaffolds are presented in Fig. 2. All the scaffolds show higher values of $\varepsilon'$ at lower frequencies, and the values decreases with increasing frequency. This behavior is due to the interfacial relaxation. The $\varepsilon'$ values of PVA-nanocomposite scaffolds are greater than the pure PVA at all frequencies due to dipole–dipole interaction on addition of nanofillers. This also shows that the dielectric properties of PVA-nanocomposites can be tuned by varying the type and concentration of nanofiller. F3 sample has higher values of $\varepsilon'$ at all frequencies among the studied samples. However, the lower values of $\varepsilon'$ of F5 may be attributed to the restriction in the mobility of polymer chains due to the introduction of $AgNO_3$-tyrosine-$TiO_2$ in the PVA matrix. This shows the inability

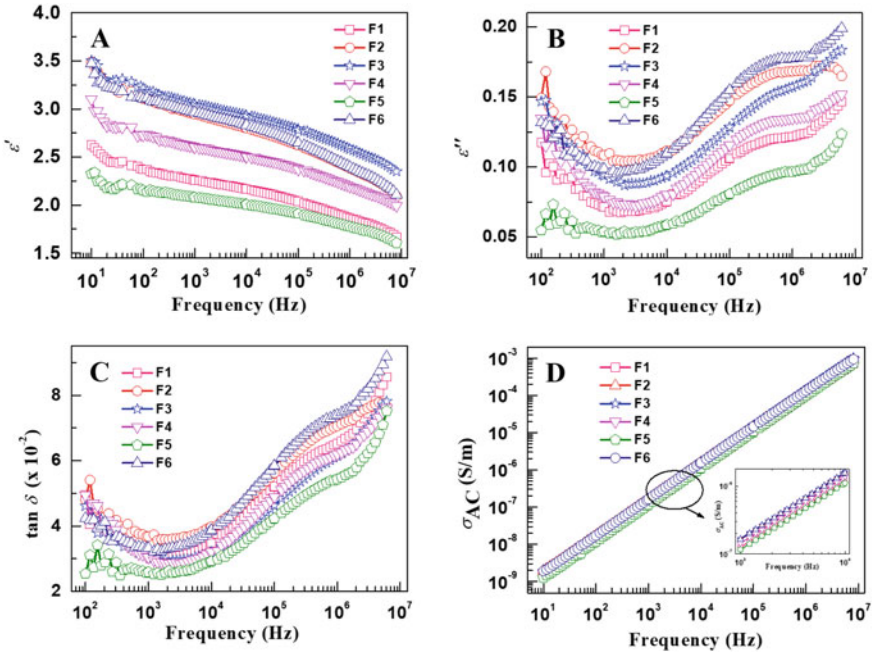


**Fig. 2** Variation in dielectric constant, $\varepsilon'$, with frequency of the pure PVA film and PVA based hybrid scaffolds (Panel A), variation in dielectric loss, $\varepsilon'$, with frequency of the pure PVA film and PVA based hybrid scaffolds (Panel B), Variation in loss tangent, tan$\delta$, with frequency of the pure PVA film and PVA based hybrid scaffolds (Panel C), and variation in AC electrical conductivity, $\sigma_{AC}$, with frequency of the pure PVA film and PVA based hybrid scaffolds (Panel D)

of polarizable units in nanocomposites to orient fast enough to keep up with the oscillations of an alternating electric field [46]. The variation of dielectric loss, $\varepsilon'$, and tangent loss, tan $\delta$, with frequency is shown in Fig. 2b, c, respectively. It can be seen that both $\varepsilon'$ and tan $\delta$ decrease with increasing frequency, reach minimum, and again increase with further increase of frequency. The higher values of $\varepsilon'$ and tanδ at higher frequencies may be due to the space charge polarization with addition of nanofillers, macroscopic distortion, and higher interfacial polarization.

The frequency dependence of AC electrical conductivity, $\sigma_{AC}$, of pure PVA and PVA-nanocomposites is shown in Fig. 2d. The $\sigma_{AC}$ increases linearly with increasing frequency of the applied electric field for all the samples. The combined effect of intrinsic dipole polarization and Maxwell–Wagner–Sillars (MWS) polarization explains the frequency dependence of $\sigma_{AC}$ [47]. The sample F6 shows relatively higher values of $\sigma_{AC}$ at all frequencies compared to the remaining composite scaffolds.

The photocatalytic degradation of malachite green in the presence of various scaffolds composition under the influence of UV light was investigated by observing the optical and spectroscopic changes in the dye solutions. The absorbance maxima in malachite green can be noted at 618 nm due to the existence of the linked benzene rings. When these benzene rings are simplified into by-products owing to the photocatalytic degradation effect by the F1-F6 films, the absorbance of the dye decreases, and therefore, the degradation of the dyes can be noted. The chemical structure of malachite green is displayed in the inset in Fig. 3a. The decrease in the absorbance is recorded, and values are represented in comparison with the original dye solution measured in time-dependent manner as shown in Fig. 3a. The malachite green was directly degraded under the UV light and was recorded as control. Other parameters that have an influence on degradation of dye are initial concentration of dyes, pH, type of photocatalyst, concentration of photocatalyst, and the reaction temperature, which were kept constant for comparison purpose [48].

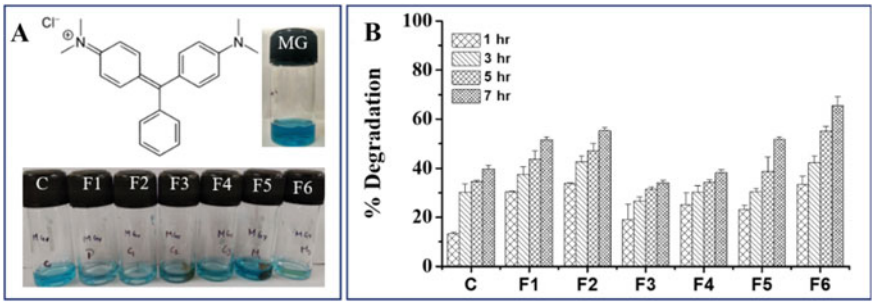


**Fig. 3** Chemical structure of malachite green (MG) dyes. The optical image of malachite green at 0 h and post-treatment with different films after 7 h (Panel A). Percentage of malachite green degradation in the presence of PVA based scaffolds under UV treatment. The error bars are representative of the standard error. The scaffold dimension used is 1 * 1 $cm^2$, and the dye concentration is 10 mg/L) (Panel B)

It is interesting to observe that the UV-irradiated dye without the treatment of the films itself degraded to ~13% in first one hour, which increased post-treatment. It is interesting to observe that after 7 h, scaffold containing photocatalyst $TiO_2$ (F2, F5, and F6) indicates higher degradation compared to those films which hold only Ag nanoparticles (F3 and F4). It is important to state that the scaffold F6 has the highest dye degradation capability, which may be attributed to photocatalyst $TiO_2$ and pre-synthesized Ag nanoparticles composition. The degradation of malachite green by F6 is also clearly seen in the optical image where the dye solution is almost clear after 7 h treatment as shown in the insert of Fig. 3a. The pre-synthesized Ag nanoparticles incorporation with $TiO_2$ and PVA (F6) has higher photocatalytic effect than pure PVA ($p < 0.05$), PVA-$Ag^+$-tyrosine ($p < 0.05$), and PVA-$TiO_2$ ($p < 0.05$). The basic mechanism of photocatalysis using $TiO_2$ under UV irradiation is well documented [32, 49–51]. When UV light falls on the $TiO_2$, electron-hole pairs are formed, and the positively charged holes encounter water molecules to produce $H^+$ and hydroxy radicals (OH·), and the negatively charged electrons react with dissolved oxygen to form superoxide ($O_2^-$) ions, which sequentially reacts with water molecules to yield hydroxide ions ($OH^-$) and peroxide radicals (OOH·). The holes oxidize $OH^-$ to OH,· and the peroxide radicals combine with $H^+$ to form OH· and $OH^-$. Due to the high energy of the UV, the recombination of the electron–hole pairs is prevented. Therefore, each species of the radicals (OH·, $OH^-$, $O_2^-$, OOH·) attacks the chromophores and degrades them [21]. The higher surface area and the lower binding energy of $TiO_2$ may be the major contributor to dye degradation. It was captivating to observe that the degradation by F3 and F4 was comparable at different hours of treatment, which indicated that the in-situ synthesized (F3) and ex-situ synthesized (F4) Ag nanoparticles could not take part efficiently in malachite green degradation. However, the degradation efficiency increased due to the collaborative efforts of Ag nanoparticles and $TiO_2$ as seen in raise in degradation efficiency in F5 and F6, respectively.

Since $Ag^+$, Ag nanoparticles, and $TiO_2$ are known to have antibacterial potential, we have further evaluated their antimicrobial capabilities toward Gram-negative bacteria (*Escherichia coli*). The antimicrobial efficiency of the polymeric scaffolds containing PVA, $AgNO_3$, $TiO_2$, tyrosine, and tyrosine-capped Ag nanoparticles is assessed in time-dependent manner, and the bacterial growth curve is constructed as shown in Fig. 4. The films containing $Ag^+$ in the formulation are found to be the most effective, and a complete inhibition in the growth of *Escherichia coli* is observed. $AgNO_3$ is a well-known for its antibacterial activity [52]; however, its usage is limited due to its extensive toxicity through bioaccumulation [53]. They exert their toxicity through depletion of glutathione and surpass the ROS capacity of the cell thereby leading to secondary damages to lipids, proteins, and DNA. Alternatively, $Ag^+$ ions also activate the Fenton reactions leading to proliferation of ROS generation [54, 55]. The Ag nanoparticles embedded in the PVA scaffolds (F4 and F6) could not control the bacterial growth, which may be attributed to the restricted dissolution of Ag nanoparticles to $Ag^+$ ions. Nevertheless, this work demonstrates that the suitable formulation of scaffolds with integration of active nanomaterials may provide opportunities in controlling industrial dye pollution, preventing the

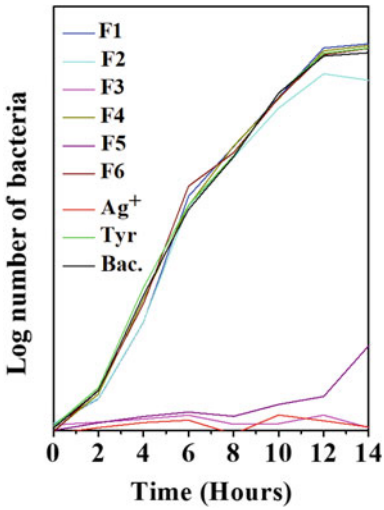


**Fig. 4** Bacterial cell growth for *Escherichia coli* after treatment with PVA based scaffolds and controls

dissemination of pathogenic bacteria, and in energy storage or flexible electronics. Such scaffolds may additionally find their utility in water remediation due to their potential as photocatalyst and antimicrobials, which needs further investigations.

## 4 Conclusions

In summary, we report formulation of various PVA scaffolds integrated with Ag nanoparticles, $TiO_2$, or reducing agent/metal ions, respectively. The importance of scaffold-integrated particles is established by investigating the dielectric properties, AC electrical conductivity, dye-degradation capacity, and antibacterial potential of these scaffolds. The results of the study suggest that appropriate homogenous amalgamation of nanoparticles or functionally active molecules within the PVA scaffolds can open new opportunities toward dye degradation, antimicrobials, energy storage, and flexible electronics.

**Acknowledgements** AU acknowledges the VRC scholarship provided by Rao Bahaddur Dharmapravartha Gubbi Thotadappa Charities, Bengaluru, India. The generous support of Japan Science and Technology (JST) Agency, Japan, toward Asia Youth Exchange Program in Science (Sakura Exchange Program) is duly accredited by AU, NPN, and HKD. Further, HKD appreciates the Centre for Advanced Materials and Industrial Chemistry (CAMIC) in the School of Sciences, RMIT University, Australia, for an Honorary Visiting Research Fellowship. SM acknowledges the contribution from Siddaganga Institute of Technology for facilitation of the project facilities. SRM wish to thank the Vision Group on Science and Technology (VGST), Department of Information Technology, Biotechnology and Science & Technology, Government of Karnataka, for providing financial support under project no. KSTePS/VGST/03/CISEE/2015-2016/GRD-470.

## References


1. Langhals H (2004) Color chemistry. Synthesis, properties and applications of organic dyes and pigments. By Heinrich Zollinger. Angewandte Chemie International Edition 43(40):5291–5292
2. Eren Z (2012) Ultrasound as a basic and auxiliary process for dye remediation: a review. J Environ Manage 104:127–141
3. Asghar A, Raman AAA, Daud WMAW (2015) Advanced oxidation processes for in-situ production of hydrogen peroxide/hydroxyl radical for textile wastewater treatment: a review. J Clean Prod 87:826–838
4. Ajmal A et al (2014) Principles and mechanisms of photocatalytic dye degradation on TiO 2 based photocatalysts: a comparative overview. RSC Advances 4(70):37003–37026
5. Kant R (2011) Textile dyeing industry an environmental hazard
6. Pandey PK et al (2014) Contamination of water resources by pathogenic bacteria. Amb Express 4(1):51
7. Joseph S, Mathew B (2015) Microwave assisted facile green synthesis of silver and gold nanocatalysts using the leaf extract of *Aerva lanata.* Spectrochim Acta Part a Mol Biomol Spectrosc 136:1371–1379
8. de Lima ROA et al (2007) Mutagenic and carcinogenic potential of a textile azo dye processing plant effluent that impacts a drinking water source. Mutat Res/Genet Toxicol Environ Mutagenesis 626(1–2):53–60
9. Schneider K, Hafner C, Jäger I (2004) Mutagenicity of textile dye products. J Appl Toxicol Int J 24(2):83–91
10. Hunger K (2007) Industrial dyes: chemistry, properties, applications. Wiley, New York
11. Srivastava S, Sinha R, Roy D (2004) Toxicological effects of malachite green. Aquat Toxicol 66(3):319–329
12. Al-Fawwaz AT, Abdullah M (2016) Decolorization of methylene blue and malachite green by immobilized *Desmodesmus sp.* isolated from north Jordan. Int J Environ Sci Dev 7(2):95
13. Al-Fawwaz A, Jacob JH (2011) Removal of methylene blue and malachite green from aqueous solutions by *Chlorella* and *Chlamydomonas* species isolated from a thermal spring environment. Int J Integr Biol 12(1):36–40
14. Mascolo G et al (2007) Photocatalytic degradation of methyl red by $TiO_2$: comparison of the efficiency of immobilized nanoparticles versus conventional suspended catalyst. J Hazard Mater 142(1–2):130–137
15. Wang H et al (2010) Photochemical growth of nanoporous $SnO_2$ at the air–water interface and its high photocatalytic activity. J Mater Chem 20(27):5641–5645
16. Yeh RY-L et al (2002) Textile wastewater treatment with activated sludge and powdered activated carbon. Int J Environ Stud 59(5):607–622
17. Alinsafi A et al (2005) Electro-coagulation of reactive textile dyes and textile wastewater. Chem Eng Process 44(4):461–470
18. Métivier-Pignon H et al (2003) Coupling ultrafiltration with an activated carbon cloth for the treatment of highly coloured wastewaters: a techno-economic study. Environ Technol 24(6):735–743
19. Bahrami M, Nezamzadeh-Ejhieh A (2015) Effect of the supported ZnO on clinoptilolite nanoparticles in the photodecolorization of semi-real sample bromothymol blue aqueous solution. Mater Sci Semicond Process 30:275–284
20. Sivamani S, Leena G (2009) Removal of dyes from wastewater using adsorption-a review. Int J Biosci Technol 2(4):47–51
21. Lazar M, Varghese S, Nair S (2012) Photocatalytic water treatment by titanium dioxide: recent updates. Catalysts 2(4):572–601
22. Mishra G, Mukhopadhyay M (2019) $TiO_2$ decorated functionalized halloysite nanotubes ($TiO_2$ @ HNTs) and photocatalytic PVC membranes synthesis, characterization and its application in water treatment. Sci Rep 9(1):4345
23. Pan D et al (2015) Efficient separation of electron–hole pairs in graphene quantum dots by TiO2 heterojunctions for dye degradation. ACS Sustain Chem Eng 3(10):2405–2413

24. Yan N, Xiao C, Kou Y (2010) Transition metal nanoparticle catalysis in green solvents. Coord Chem Rev 254(9–10):1179–1218
25. Navya P, Daima HK (2016) Rational engineering of physicochemical properties of nanomaterials for biomedical applications with nanotoxicological perspectives. Nano Convergence 3(1):1
26. Karak N (2019) Fundamentals of nanomaterials and polymer nanocomposites. In: Nanomaterials and polymer nanocomposites. Elsevier, pp 1–45
27. Xiong Z et al (2010) Photocatalytic degradation of dyes over graphene–gold nanocomposites under visible light irradiation. Chem Commun 46(33):6099–6101
28. Karak N, Konwarh R, Voit B (2010) Catalytically active vegetable-oil-based thermoplastic hyperbranched polyurethane/silver nanocomposites. Macromol Mater Eng 295(2):159–169
29. Murugadoss A et al (2009) 'Green'chitosan bound silver nanoparticles for selective C–C bond formation via in situ iodination of phenols. J Mol Catal a: Chem 304(1–2):153–158
30. Senthilraja A et al (2014) Synthesis, characterization and catalytic activity of co-doped Ag–Au–ZnO for MB dye degradation under UV-A light. Mater Sci Semicond Process 22:83–91
31. Saha S, Wang J, Pal A (2012) Nano silver impregnation on commercial $TiO_2$ and a comparative photocatalytic account to degrade malachite green. Sep Purif Technol 89:147–159
32. An T et al (2011) Photocatalytic degradation kinetics and mechanism of antivirus druglamivudine in $TiO_2$ dispersion. J Hazard Mater 197:229–236
33. Stapleton DR et al (2010) On the kinetics and mechanisms of photolytic/$TiO_2$-photocatalytic degradation of substituted pyridines in aqueous solutions. Appl Catal B 95(1–2):100–109
34. Daima HK et al (2011) Tyrosine mediated gold, silver and their alloy nanoparticles synthesis: antibacterial activity toward gram positive and gram negative bacterial strains. In: 2011 international conference on nanoscience, technology and societal implications. IEEE.
35. Shubha A, Manohara S, Gerward L (2017) Influence of polyvinylpyrrolidone on optical, electrical, and dielectric properties of poly (2-ethyl-2-oxazoline)-polyvinylpyrrolidone blends. J Mol Liq 247:328–336
36. Gaaz T et al (2015) Properties and applications of polyvinyl alcohol, halloysite nanotubes and their nanocomposites. Molecules 20(12):22833–22847
37. Khanna P, Singh N, Charan S (2007) Synthesis of nano-particles of anatase-$TiO_2$ and preparation of its optically transparent film in PVA. Mater Lett 61(25):4725–4730
38. Liufu S, Xiao H, Li Y (2005) Adsorption of poly (acrylic acid) onto the surface of titanium dioxide and the colloidal stability of aqueous suspension. J Colloid Interface Sci 281(1):155–163
39. Gaikwad AV, Rout TK (2011) In situ synthesis of silver nanoparticles in polyetherimide matrix and its application in coatings. J Mater Chem 21(4):1234–1239
40. Daima HK et al (2014) Synergistic influence of polyoxometalate surface corona towards enhancing the antibacterial performance of tyrosine-capped Ag nanoparticles. Nanoscale 6(2):758–765
41. Selvakannan PR et al (2013) Probing the effect of charge transfer enhancement in off resonance mode SERS via conjugation of the probe dye between silver nanoparticles and metal substrates. Phys Chem Chem Phys
42. Dubey K et al (2015) Tyrosine- and tryptophan-coated gold nanoparticles inhibit amyloid aggregation of insulin. Amino Acids 47(12):2551–2560
43. Monnappa S et al (2017) Influence of amino acid corona, metallic core and surface functionalization of nanoparticles on their in-vitro biological behaviour. Int J Nanotechnol 14(9/10/11):816–832
44. Chou H et al (2014) Interactions between silver nanoparticles and polyvinyl alcohol nanofibers. AIP Adv 4(8):087111
45. Flores C et al (2010) Spontaneous adsorption of silver nanoparticles on Ti/$TiO_2$ surfaces. Antibacterial effect on *Pseudomonas aeruginosa*. J Colloid Interface Sci 350(2):402–408
46. Huang J et al (2005) Cubic silsesquioxane–polyimide nanocomposites with improved thermomechanical and dielectric properties. Acta Mater 53(8):2395–2404

47. Ramesan MT (2015) Processing characteristics and mechanical and electrical properties of chlorinated styrene–butadiene rubber/fly ash composites. J Thermoplast Compos Mater 28(9):1286–1300
48. Reza KM, Kurny A, Gulshan F (2017) Parameters affecting the photocatalytic degradation of dyes using $TiO_2$: a review. Appl Water Sci 7(4):1569–1578
49. Medana C et al (2011) Multiple unknown degradants generated from the insect repellent DEET by photoinduced processes on $TiO_2$. J Mass Spectrom 46(1):24–40
50. Sirtori C et al (2009) Solar photocatalytic treatment of quinolones: intermediates and toxicity evaluation. Photochem Photobiol Sci 8(5):644–651
51. Lu C-S et al (2009) Identification of the degradation pathways of alkanolamines with $TiO_2$ photocatalysis. J Hazard Mater 165(1–3):306–316
52. Feng QL et al (2000) A mechanistic study of the antibacterial effect of silver ions on Escherichia coli and Staphylococcus aureus. J Biomed Mater Res 52(4):662–668
53. Bouwmeester H et al (2011) Characterization of translocation of silver nanoparticles and effects on whole-genome gene expression using an in vitro intestinal epithelium coculture model. ACS Nano 5(5):4091–4103
54. Palza H (2015) Antimicrobial polymers with metal nanoparticles. Int J Mol Sci 16(1):2099–2116
55. Matur M et al (2020) *Engineering bioactive surfaces on nanoparticles and their biological interactions.* Sci Rep 10:19713